Preclinical Evaluation of Fluorine-18-Labeled Androgen Receptor Ligands in Baboons

Thomas A. Bonasera, James P. O'Neil, Ming Xu, Jeffrey A. Dobkin, P. Duffy Cutler, Lennis L. Lich, Yearn Seong Choe, John A. Katzenellenbogen and Michael J. Welch

Mallinckrodt Institute of Radiology, Washington University School of Medicine; Department of Chemistry, Washington University, St. Louis, Missouri; and Department of Chemistry, University of Illinois, Urbana, Illinois

A noninvasive method for detecting and quantifying androgen receptors (AR) in metastatic prostate cancer may be helpful in choosing the method of treatment and in better understanding the pathophysiology of this disease. Nine previously synthesized fluorinated androgens exhibited high affinity binding to AR and showed AR-mediated uptake in the ventral and dorsal prostate of the rat. Further evaluation of these agents for PET imaging is needed since sex hormone binding globulin (SHBG), a glycoprotein which binds androgens with high affinity, is absent in rat blood but is present at high levels in the blood of primates. We chose to study three of the nine fluoro-androgens by PET in the baboon. **Methods:** In this study, 16β-[^{18}F]fluoro-5α-dihydrotestosterone (**I**), 16β-[^{18}F]fluoromibolerone (**II**) and 20-[^{18}F]fluoromibolerone (**III**) were synthesized and studied in both a young and old male baboon using PET. Blood samples were withdrawn in three of the 10 studies and analyzed for total radioactivity and percent unmetabolized radioligand. Tissue radioactivity was evaluated semiquantitatively, using prostate absolute, standard and target to nontarget uptake values. **Results:** Prostate uptake was observed with all three ^{18}F-androgens. At 60 min postinjection, compound **I** gave the highest prostate to soft tissue ratios in both baboons and prostate uptake was shown to be AR-mediated by blocking uptake through the coadministration of testosterone. Compound **I** gave the highest level of unmetabolized radioligand present in blood up to 45 min postinjection, and gave a 37-fold greater prostate-to-bone ratio at 2 hr postinjection in baboons compared to rats. The favorable behavior of this compound in the baboon may be related to its high affinity for SHBG. **Conclusion:** All three compounds can be used to determine AR-positive tissue in primates. Compound **I** was selected for the evaluation of AR in men with prostate cancer using PET.

Key Words: prostate cancer; positron emission tomography; androgen receptor; 5α-dihydrotestosterone; mibolerone

J Nucl Med 1996; 37:1009–1015

Prostate cancer kills more than 40,000 men in the United States annually (*1*). Most prostate cancers express the androgen receptor (AR) and show an initial response to hormonal therapy. However, most cases eventually become hormone independent, through a mechanism that, as yet, is unknown. Noninvasive imaging of AR may help to clarify how these tumors become hormone independent (*2*) and may illuminate the basic biology of this disease.

While the presence of AR in patients in prostatic cancer may be helpful in suggesting a course of endocrine therapy (*3–13*), the correlation between AR positivity and response to therapy is not as good as that between estrogen and progesterone receptor positivity and response to antihormonal (e.g., tamoxifen) therapy in breast cancer (*3,8,9*). This poor correlation in prostate cancer has been attributed to under sampling (*3*), and to AR heterogeneity (*14*). Visualization of AR in the tumor using an AR-based imaging agent might provide a better representation of the AR status of the tumor. Except for treatment with the antiandrogen flutamide (*15*), such AR-based imaging could be followed throughout hormonal therapy, as other common hormonal therapies (bilateral orchiectomy, administration of estrogenic compounds such as diethylstilbestrol, aminoglutethimide, ketoconazole or a luteinizing hormone-releasing hormone (LHRH) agonist) would be expected to leave the AR unoccupied (*16–20*). AR-based imaging of prostate cancer patients on such hormone regimens might be particularly interesting, based on the recent report that the AR gene itself may become amplified many fold in this disease (*21*).

Several AR ligands have been labeled with the positron-emitting nuclides fluorine-18 (*22–24*) and carbon-11 (*25,26*), and with radioisotopes of bromine (*27,28*), iodine (*29–33*) and selenium (*34*). We have evaluated nine fluorinated androgens (*22–24*) with high in vitro affinity for the androgen receptor in a rat model (*35*). All ligands exhibited high in vivo AR-mediated, limited capacity uptake into the ventral and dorsal prostate of the rat. These compounds do differ rather significantly in their binding affinity for the progesterone receptor (PgR) and for sex-hormone binding globulin (SHBG). In principle, the binding of an AR-based prostate imaging agent to PgR is undesirable, since prostate tumors are known to contain PgR (*2,36–39*).

SHBG is a steroid-binding glycoprotein found in the blood of primates, but not mature rats (*40,41*). While we have previously suggested that an AR ligand should be designed to have low affinity for SHBG to improve its imaging characteristics (*22–24,35,42,43*), recent evidence has implicated the SHBG in both the protection of androgens and estrogens from metabolism (*40,44*) and in the facilitation of their uptake into target tissues (*45*). In fact, a receptor for SHBG has been found on the surface of both prostate (*46,47*) and prostate cancer (*48*) cells, indicating that SHBG may have a role in transporting sex steroid from the blood into target cells.

We evaluated our fluorine-18-labeled AR ligands in the male baboon using PET because the caudal prostate of the baboon has been shown to be histologically and pharmacologically similar to the human peripheral prostate (*49*), the tissue in which most human prostate cancers arise (*50*). Three fluorine-18 androgens, 16β-[^{18}F]fluoro-5α-dihydrotestosterone, 16β-[^{18}F]FDHT, **I**, 16β-[^{18}F]fluoromibolerone, 16β-[^{18}F]Fmib, **II** and 20-[^{18}F]fluoromibolerone, 20-[^{18}F]Fmib, **III**, were selected for this study. Pertinent data (*23,24,43*) on these three compounds are summarized in Table 1.

Compound **I**, a derivative of the endogenous androgen DHT, has high affinity for rat AR and very high affinity for SHBG; it also has the lowest PgR affinity of those measured. By contrast,

Received May 30, 1995; revision accepted Oct. 20, 1995.

For correspondence or reprints contact: Michael J. Welch, PhD, Mallinckrodt Institute of Radiology, Washington University School of Medicine, 510 S. Kingshighway Blvd., St. Louis, MO 63110.

TABLE 1
Selected Relative Binding Affinity (RBA) and Rat Biodistribution Data for Compounds I, II and III*

Compound	RBA for AR	RBA for PgR	RBA for SHBG	1 hr Rat prostate uptake (%ID/g)	4 hr Rat prostate-to-muscle ratio
16β-[^{18}F]Fluoro-5α-dihydrotestosterone (I)	42.7	0.12	385	0.432	24.87
16β-[^{18}F]Fluoromibolerone (II)	30.8	3.0	1.3	0.667	10.91
20-[^{18}F]Fluoromibolerone (III)	53.2	43.7	4.0	0.969	13.25

*Data are from references (*14–16*). Reference ligands (K_d in n*M*) are R1881 (0.6), R5020 (0.4) and estradiol (1.6) for AR, PgR and SHBG, respectively. Prostate uptake shown is for the ventral lobe.

compounds **II** and **III** derivatives of mibolerone, have high affinity for the rat AR but low affinity for SHBG. The large difference in SHBG affinity between compound **I** and compounds **II** and **III** may reveal the effect that this blood protein has an androgen uptake into target tissues and on stability toward metabolism. The affinity of compounds **II** and **III** for PgR is also higher than that of compound **I**. The location of the fluorine label on derivative **III** is at the C-20 position (on the C-20 methyl group). This contrasts with the C-16β-fluorine location (on the steroid D-ring) on both compounds **I** and **II**. Using these compounds we can also investigate whether the positron of fluoride substitution affects the rate of metabolic defluorination in the primate, as indicated by bone uptake.

MATERIALS AND METHODS

Radiochemical Synthesis

Compounds **I**, **II** and **III** were prepared as previously described (*23,24*) starting with 200 to 400 mCi aqueous [^{18}F]fluoride immediately after cyclotron bombardment. The final product, purified by normal phase HPLC, was evaporated to dryness in vacuo and redissolved in 1:9 ethanol:normal saline. Radiochemical yields were similar to those previously reported and specific activity in all cases was >600 Ci/mmole. The yields and specific activities of compound **I** were significantly greater than for compounds **II** and **III**. The final solution was sterile-filtered through a prewetted filter prior to injection into the baboon. For every preparation radiochemical purity was determined to be >95% by analytical reversed phase HPLC (C-18, 0.46 × 25 cm, Alltech, Deerfield, IL, 1:1 water:acetonitrile, 1 mL/min) and effective specific radioactivity was determined by an in vitro competitive androgen receptor binding assay using isolated rat AR and [^{3}H]R1881 as adapted from a published procedure (*51,52*). The radioactivity injected in each study ranged from 2.4 to 6.9 mCi. Carbon-15-oxygen was used as a tracer to determine the position of blood vessels. This was prepared as previously described (*53*).

Animals

Two male baboons (Papio papio) were caged and allowed free access to food and water up to approximately 18 hr prior to injection of tracer. Baboon 1 weighed 29.5 kg and was approximately 18 yr old, while Baboon 2 weighed 16.8 kg and was approximately 6 yr old. The anesthetized baboons (400–550 mg ketamine; 0.4 mg atropine sulfate) were injected intravenously with the tracer solution in a vein of either the hind- or foreleg. The animals were placed supine in a u-shaped acrylic holder and were maintained on saline (500–750 ml total) over the course of the study. The animals were administered pentobarbital (400–650 mg total) periodically during the experiment when they responded by blinking to a gentle stream of air to the eye area. In an additional study, Baboon 1 was co-administered testosterone (10.2 mg, 35.4 μmol) with radiotracer **I** to observe whether prostate uptake was receptor-mediated and thus saturable. In three studies, one with each compound, blood samples were obtained. In two studies with compound **I**, urine was removed from the animal via catheter at two different times. All animal experiments were carried out in compliance with the guidelines for the care and use of research animals established by Washington University's Animal Studies Committee.

PET Imaging

PET imaging was performed with the PETT VI (six studies, all three androgens in each of the two baboons) (*54,55*), the Siemens/CTI ECAT EXACT 921 (two studies on Baboon 1 with compound **I**, one of which was a blocking experiment) or the Siemens/CTI ECAT 953b (two studies, one on each baboon, with compound **III**) scanner.

The PETT VI device permits the simultaneous acquisition of seven transverse tomographic slices, with a slice-to-slice separation of 1.44 cm, a slice thickness of 1.39 cm and a reconstructed resolution of 12.0 mm (FWHM). The Siemens/CTI ECAT EXACT 921 is a whole-body device that acquires 47 simultaneous slices of ≈3.4 mm (FWHM) over an axial distance of 16.2 cm. This tomograph has a best-case reconstructed spatial resolution of 5.5 mm (FWHM) in both the axial and transaxial directions. Reconstructed spatial resolution under imaging conditions is approximately 8 mm (FWHM). The Siemens/CTI ECAT 953b acquires 31 simultaneous slices at a section interval of approximately 3.4 mm over an axial extent of 10.6 cm. The 953b has spatial resolution better than 6.6 mm in both the axial and transaxial directions. With each study, a 10–15 min transmission scan was performed using a ^{68}Ge/^{68}Ga source, prior to tracer injection and collection of initial emission scans.

MRI

The baboons were imaged on a 1.5 T Siemens MAGNETOM MRI device. The animals were anesthetized and unconscious as described above. While several scanning sequences were used, only the T2-weighted images are presented in the results.

Analysis of PET Data

All data were corrected to the time of tracer injection. ROIs were typically obtained using isodensity contours on transaxial slices. For the PETT VI and Siemens/CTI ECAT 953b studies, prostate and bladder were defined at the 60 and 90 min time points, respectively. Tissue ROIs were defined as the average of several circular regions, representing muscle or another soft tissue. Blood ROIs were defined from images obtained following the inhalation of C^{15}O (*56*) and represent the femoral vessels. Bone ROIs were defined from transmission scans.

For the Siemens/CTI ECAT EXACT 921 studies, all ROIs were defined by observation of the projected, three-dimensional rendered images. A maximum pixel value method was used to determine androgen receptor mediated and urinary associated uptake, eliminating partial volume sampling errors (*57*). These

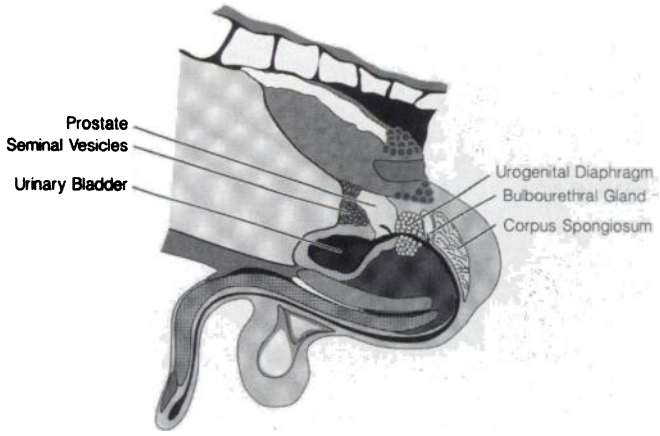

FIGURE 1. Drawing of sagittal view of baboon pelvic region indicating the proximity of the prostate in relation to the bladder (*59*).

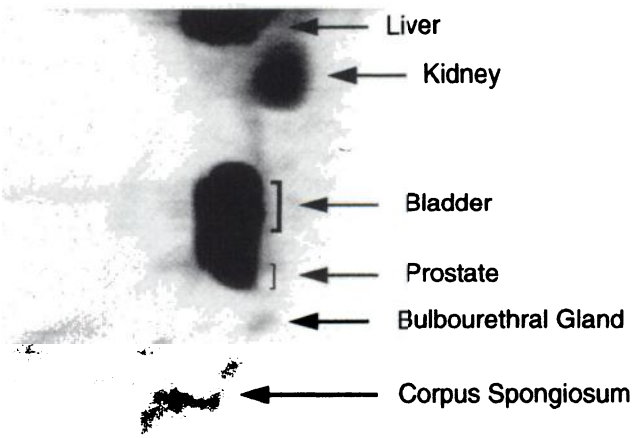

FIGURE 2. Projected, three-dimensional rendered image of compound **I** in Baboon 1, as obtained from the Siemens/CTI ECAT EXACT 921 scanner. Tissues of interest are indicated with arrows. The prostate is located at the base of the large area of increased radioactivity in the center of the image of which the rest is bladder.

values were converted to differential uptake ratio (DUR) using the scanner's automated calibration function and the body weight of the baboon (*58*).

The validity of these ROIs was confirmed by comparison to published information on baboon anatomy (*57,58*), as adapted in Figure 1, and to MR images of the two baboons used in this study.

Blood Analysis

Blood samples were withdrawn from Baboon 1 following injection of radioandrogens **I**, **II** and **III**. Immediately after withdrawal, approximately 0.2 ml blood was delivered to a preweighed glass vial for determination of percent injected dose radioactivity per gram of (%ID/g). Another 0.2 ml blood was delivered to a plastic centrifuge tube containing 0.2 ml absolute ethanol for extractive fractionation and chromatographic determination of unmetabolized radioligand. Blood processing consisted of vigorous mixing for 2 min followed by centrifugation at 27,000 G for 45 min. The ethanolic fraction was spotted on a 5 × 20-cm silica TLC plate (Redi/Plate silica gel G, Fisher Scientific, Pittsburgh, PA) and developed in 2:1 ethyl acetate:hexane. Analysis was performed on a radio-TLC scanner (System 200 Imaging Scanner, Bioscan, Washington, DC). Data for these blood analyses are presented as percent extractable, unmetabolized radioligand:

$$\text{Extractable, unmetabolized radioligand} = (\%\text{ID/g}) \times (\text{fraction in ethanolic supernatant}) \times (\text{fraction unmetabolized by TLC}).$$

RESULTS

Baboon PET Studies and Blood Analysis

Typical PET images using both the high-resolution ECAT scanner and PETT VI are shown in Figures 2–4. Figure 2 shows an ECAT EXACT-projected three-dimensional rendered image of compound **I** in Baboon 1. In spite of the high uptake in the bladder, kidney and liver, the areas of specific uptake are clearly visualized. Figure 3 displays for both baboons the correlation of the PETT VI images of compound **I** with MR images. Figure 4 shows an ECAT EXACT 921 image of compound **I** exhibiting specific uptake in AR-containing tissues inferior to the prostate.

Prostate uptake data for all three compounds, as determined by PETT VI, is shown in Table 2. The prostate to nontarget (tissue, blood and bone) activity ratios determined from PETT VI data at 60 min are shown in Figure 5 for all experiments, except that in which compound **II** was injected into Baboon 2, which is presented at 30 min postinjection. Blood metabolism data, presented as % ID/g unmetabolized compound, are plotted versus time in Figure 6.

Compound I: For both animals, PETT VI prostate uptake of compound **I** gave absolute values greater than 0.4 PETT VI counts/voxel/sec/mCi, from 15 min through 90 min postinjection. Prostate to bone values remained above 3 from 30 min to 90 min postinjection for Baboon 2, and remained above 5 for the older baboon during the same time period. Prostate to soft tissue values greater than 6.5 were observed for both baboons at 60 min, and a prostate to blood value of greater than 3.5 was observed in the older baboon at 60 min postinjection.

Because of its favorable characteristics, compound **I** was studied further using the higher resolution ECAT EXACT 921. Scanning of Baboon 1 after injection of high-effective specific radioactivity **I**, resulted in prostate DUR of between approximately 25 and 30 from 40 to 60 min postinjection, as shown in Figure 7. Withdrawal of urine activity via catheter at 118 min postinjection caused bladder DUR values to drop dramatically, from a range of approximately 48–55 prior to withdrawal to a value of 28 post; prostate DUR values actually increased after withdrawal of urine. A second removal of urine from the

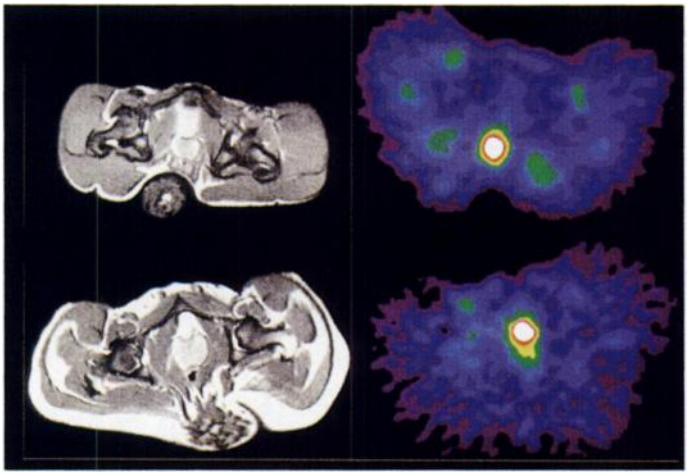

FIGURE 3. Comparison of transaxial images obtained with MRI (left, gray scale) to those obtained 60 min after injection of compound **I** with PETT VI (right, color). Upper images are of Baboon 2; lower are of Baboon 1. The medially located medium gray area in the MR images and the white area of increased radioactivity in the PET images is the prostate.

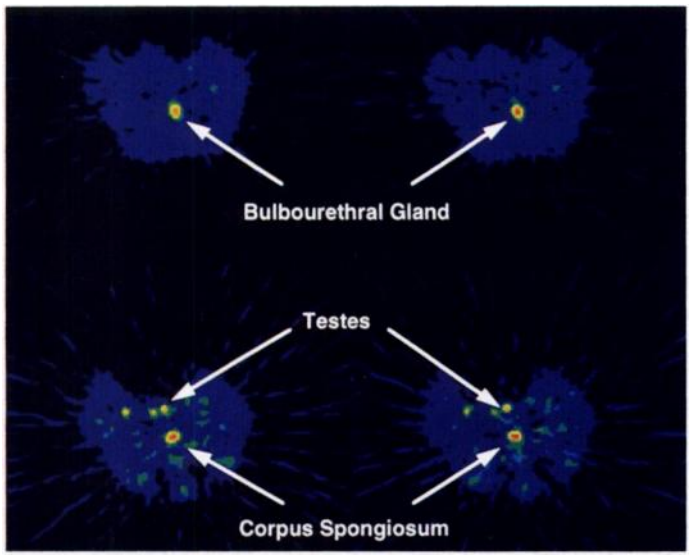

FIGURE 4. Siemens/CTI ECAT EXACT 921 transaxial images of tissues inferior to the prostate which are known to contain AR: bulbourethral gland and corpus spongiosum. Images obtained using compound **I** in Baboon 1. Testicular uptake is also observed as compound **I** is expected to cross the blood–testicle barrier.

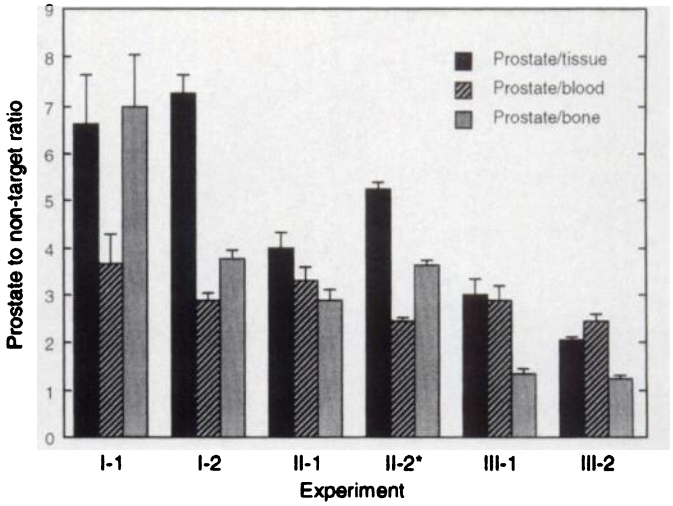

FIGURE 5. PETT VI target to nontarget ratios for compounds **I**, **II** and **III** in Baboons 1 and 2 at 60 min postinjection. The soft-tissue value was determined using several circular regions of low uptake surrounding the prostate which represent muscle and other soft tissue. Errors shown are the standard deviation of the pixel counts included in the region. *Ratios for compound II in Baboon 2 are shown for 30 min postinjection due to a technical problem with the 60-min data.

baboon at 290 min caused bladder DUR to drop to 10, while prostate radioactivity remained constant.

As expected, injection of testosterone with **I** gave prostate DUR well below 10 at 20–40 min, as observed on the ECAT EXACT 921 (Fig. 7). As before, removal of 22.9% ID as urine at 120 min resulted in a drop in bladder DUR from a maximum of over 35 at 40 min to less than 10 at 140 min postinjection.

Compound II: Prostate uptake of **II** in Baboon 1 was between 0.2 and 0.27 PETT VI counts/voxel/sec/mCi from 15 min to 60 min postinjection and increased to greater than 0.5 at 90 and 120 min. In the younger baboon, uptake was erratic and remained below 0.4 through 60 min, but was greater than 1.2 at 90 to 120 min. At 120 min, this compound gave prostate to bone ratios of 10 for Baboon 1. The level of 0.005% ID/g unmetabolized **II**, present in blood at 2 min, decreased gradually to less than 0.002% ID/g at 30 min postinjection (Fig. 6).

Compound III: Prostate uptake for compound **III** in Baboon 1 remained at or below 0.21 PETT VI counts/voxel/sec/mCi for the duration of the 120-min experiment. Uptake in Baboon 2 was between 0.36 and 0.38 from 15 to 60 min postinjection, and increased to greater than 0.5 by 120 min. At 60 min, prostate to soft tissue and prostate to blood ratios were between 2 and 3 for both animals, and prostate to bone ratios were near unity.

This compound was also studied in the higher resolution ECAT 953b. Prostate to soft tissue and prostate to blood activity ratios ranged from 6 to 9 at 60 min. At this time, the prostate to bone ratio in this scanner was near 3 for the older baboon and near 5 for the younger baboon. A comparison of prostate to nontarget ratios, determined by PETT VI and ECAT 953b, is shown for compound **III** in both baboons in Figure 8. As with **II**, the unmetabolized compound was initially present in blood at 0.005% ID/g; this value decreased rapidly to nearly undetectable levels after 30 min (Fig. 6). All activity in the blood was present as metabolites.

Anatomy and Uptake

Although the primate prostate is close to other tissues containing high levels of radioactivity such as the bladder, we ascertained that the regions defined as prostate are, in fact, prostate and that the uptake of radioactivity in these regions is mediated by the androgen receptor through several observations: (a) in the PETT VI experiments, the time-activity curves for compound **I** in both baboons indicated that the region defined as prostate (through comparison to MR images (Fig. 3) and published baboon anatomy (Fig. 1)) exhibited uptake which increased to a peak or a plateau in 30 to 90 min, as expected for an androgen-receptor mediated process; (b) the site of this activity was immediately inferior to tissue which exhibited

TABLE 2
Prostate Radioactivity Following Administration of Radioandrogens **I-III** in Baboons 1 and 2 as Measured with PETT VI*

Time (min)	Compound I		Compound II		Compound III	
	Baboon 1	Baboon 2	Baboon 1	Baboon 2	Baboon 1	Baboon 2
0	0.11	0.24	0.33	0.22	0.16	0.24
15	0.41	0.41	0.20	0.21	0.18	0.36
30	0.42	0.46	0.21	0.38	0.20	0.38
60	0.44	0.47	0.27	†	0.19	0.38
90	0.40	0.42	0.59	†	0.21	0.43
120	0.39	0.24	0.55	†	0.17	0.51

*Prostate region was defined with an isodensity contour. Radioactivity is for one transaxial slice normalized to amount of tracer injected and is reported in the units PETT VI counts/voxel/sec/mCi.

†No data due to image reconstruction problems.

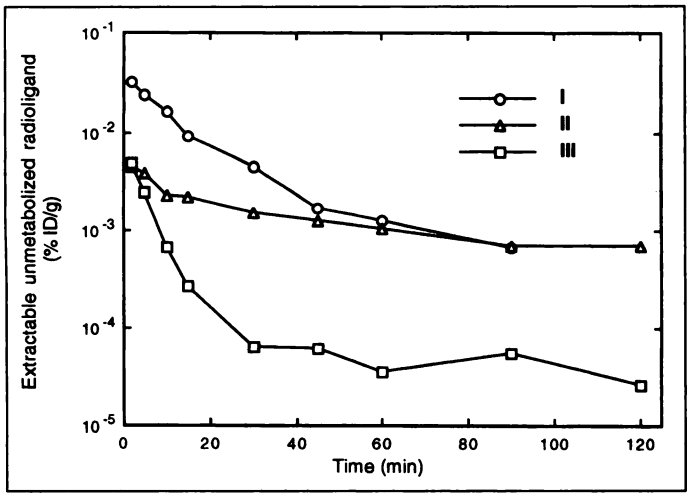

FIGURE 6. Semi-logarithmic plot versus time of blood unmetabolized, ethanol extractable radioligand for the three compounds in Baboon 1.

extremely high and progressively increasing uptake, which clearly was bladder; (c) in the ECAT EXACT experiment in which high-effective specific radioactivity **I** was delivered to Baboon 1, removal of urine twice via catheterization caused a 50% decrease in bladder radioactivity, while prostate activity increased slightly, thereby indicating that the region defined as prostate is not simply image spillover from urinary radioactivity; (d) the testosterone-blocking experiment performed on the ECAT EXACT scanner resulted in a 70% drop in prostate DUR, suggesting that the prostate uptake is limited capacity and androgen receptor mediated (Fig. 7) and, as in all other studies, increasing uptake in the bladder was observed even with testosterone blocking. Our studies do not rule out the possibility that the added testosterone blocks SHBG binding and so dramatically increases metabolism of compound **I**.

Other androgen receptor-containing tissues in the baboon, the bulbourethral gland (BG) and the corpus spongiosum (CS), which lie inferior to the prostate, show increased uptake of radioactivity. These structures can be seen in Figure 1. While in the hamster the BG has been shown to contain abundant AR (*60*), the CS has been shown to contain low levels of AR in mature mammals (*61,62*) and is thus not likely to be a target site for PET. Qualitative analysis of the time-activity curves for these regions in the compound **I** experiments indicated that the radioactivity observed is clearly distinguishable between blood pool, AR-associated and urine (data not shown). Blood pool activity, as defined from $C^{15}O$ scans, gradually drops off from among the highest levels of all the tissues initially, to among the lowest levels at the final time point in both baboons. AR-associated activity in the prostate and other target sites such as the BG increased to a peak near 60 min in both baboons with the younger baboon's AR-mediated uptake dropping to near blood levels shortly after 60 min, with the drop being more gradual in the older baboon. The rate of accumulation of urinary activity was somewhat variable, but bladder activity reached high levels.

Although all three compounds showed similar prostate uptake (as measured in PET units), compound **I** showed high absolute uptake (Table 2) and the highest prostate to soft tissue ratio. Using the higher resolution ECAT EXACT 921 scanner, we could demonstrate that a blocking dose of unlabeled testosterone caused a 70% drop in the prostate and BG activity, suggesting that the compound uptake is AR-mediated. All urogenitary regions in several slices were evaluated on a maximum pixel radioactivity basis (to eliminate partial volume sampling) (Fig. 9). No decline was seen in CS activity, which appears to be near the level of that of the blood pool, consistent with the low levels of AR in this tissue (*61,62*).

The comparison of the prostate to nontarget ratios for compound **III** on the PETT VI scanner versus those on the higher resolution Siemens ECAT 953b scanner indicated the advantages of the higher resolution instrument (Fig. 8). An organ the size of a walnut in humans, the baboon prostate is small enough to cause partial volume errors. The prostate to nontarget ratios in the lower resolution PETT VI studies with **III** were on the order of two- to six-fold lower than those obtained with the ECAT 953b.

Metabolic Stability and SHBG Affinity

A time-activity plot comparing the amount of compounds **I**, **II** and **III** that are present in the blood in an unmetabolized, extractable form, are shown in Figure 6. Initially, compound **I** was present unmetabolized in blood at a level six-fold higher than either **II** or **III**, and it remained higher than the mibolerone derivatives up to 30 min after the time of injection. Thus, at least as far as we have examined, there is a positive correlation between a compound's affinity for SHBG (Table 1) and its metabolic stability in the blood of primates; this stability may lead to increased uptake of compound **I** into AR-rich target tissues.

We cannot determine through these studies whether the high SHBG binding of compound **I** plays a more direct role in its higher level of prostate uptake, as suggested by some studies in animals and in cell culture (*45–48*). The prostate to bone uptake ratios at 2 hr postadministration are presented in Figure 9, together with the ratios obtained in a previously published biodistribution study in the rat (*23,24*). There are major species differences in these uptake ratios: Compound **I** exhibited a 37-fold increase in prostate-to-bone ratio in the baboon compared to the rat, while the ratio for compound **II** increased only 8-fold in the baboon; the ratio for compound **III** in the baboon decreased slightly, to one half of that observed in the rat. Since bone uptake of ^{18}F is thought to be indicative of the metabolic release of [^{18}F]fluoride ion, the increased prostate to bone ratios for compounds **I** and **II** in the baboon implies that

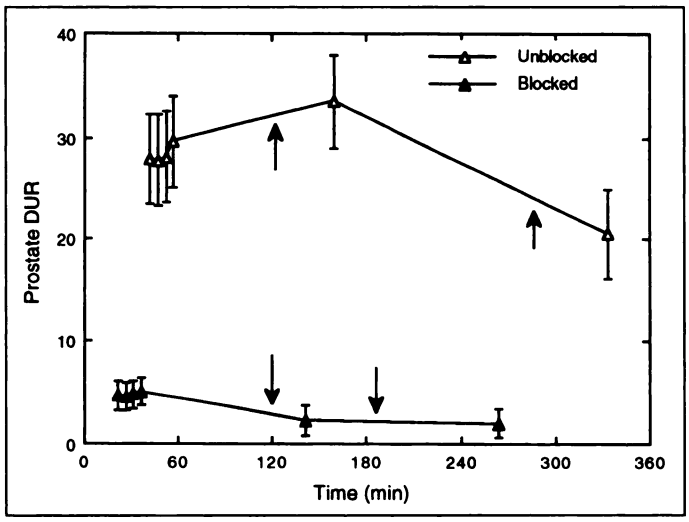

FIGURE 7. Maximum pixel analysis of the uptake of radioactivity into the prostate of Baboon 1 following injection of **I** with (blocked) or without 10.2 mg testosterone as measured with the Siemens/CTI ECAT EXACT 921 scanner. The error bars represent the maximum error for a time point within a data set. In the unblocked experiment urine was removed (indicated by arrows) via bladder catheterization at 118 min (22.3% ID) and 290 min (13.4% ID) postinjection of tracer; in the blocked experiment urine was removed at 120 min (22.9% ID) and 184 min (7.8% ID).

there is less defluorination of the 16β-fluorinated steroids in the baboon. The difference in prostate to bone uptake ratio for **I** as compared to **II** may be attributable to its higher SHBG affinity, as described above.

These baboon experiments give us an appreciation of the limitations of the rat biodistribution model for the evaluation of androgens as potential imaging agents in man. Without the presence of serum SHBG, androgen receptor ligands with structural features that reduce metabolism (e.g., 17α-methyl substitution) and increase the affinity for rat AR, give higher prostate uptake in the rat than do derivatives of the endogenous ligands T or DHT, regardless of the compound's affinity for SHBG. Thus, the male rat model does not predict the target uptake of androgens expected in primates quantitatively.

Our findings also suggest that in addition to high AR binding affinity, high SHBG affinity is also desirable for AR imaging agents. The beneficial effect of SHBG binding that we observed on target tissue uptake and selectivity in this study may also account for an apparent curiosity we have encountered recently in PET imaging of estrogen receptors in human female breast cancer patients with 16β-[^{18}F]fluoromoxestrol (βFMOX) (*63,64*). βFMOX has the highest ER-mediated target uptake in rats (*63,64*) of more than 20 radioestrogens studied, and its affinity for SHBG is 256 times lower than that of 16α-[^{18}F]fluoroestradiol (FES) (*51,65*), the agent being used for PET estrogen receptor imaging (*66–68*). Nevertheless, our experience with βFMOX to date in humans, has been disappointing (Dehdashti F, Siegel BA, Bonasera TA, Katzenellenbogen JA, Welch MJ, *personal communication*, 1995) we have been unable to detect ER-positive (ER+, greater than 3 fmol/mg protein) breast cancer in three patients with known ER+ status (as determined by ex vivo ER assays on a biopsy sample) and βFMOX also exhibited high uptake into the blood vessel into which it was injected. Both phenomena could be attributed to the low affinity βFMOX has for SHBG (*69*).

CONCLUSION

All three androgens studied showed specific uptake in the baboon prostate. A combination of ease of synthesis and superior target to nontarget tissue ratios led us to select compound **I**, 16β-[^{18}F]fluoro-5α-dihydrotestosterone, for the evaluation of AR in men with metastatic prostate cancer.

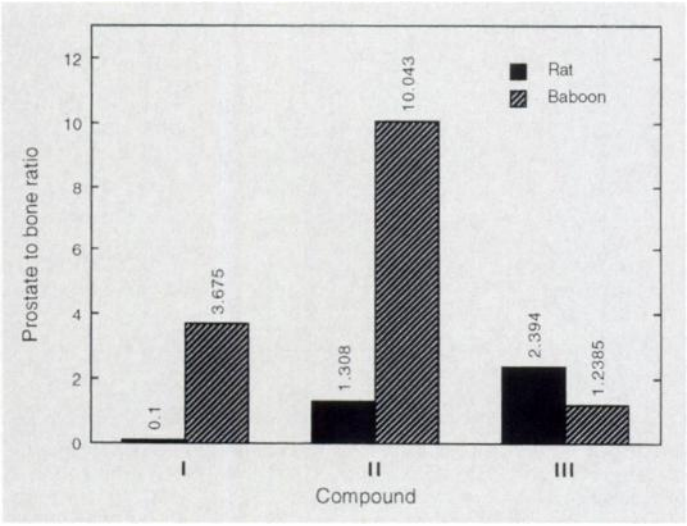

FIGURE 8. Comparison of 2 hr postinjection rat (*23,24*) and baboon prostate to bone ratios for compounds **I**, **II** and **III**. Baboon data are from PETT VI studies and represent the average of the values obtained from Baboons 1 and 2 for compounds **I** and **III**, or for Baboon 1 for compound **II**.

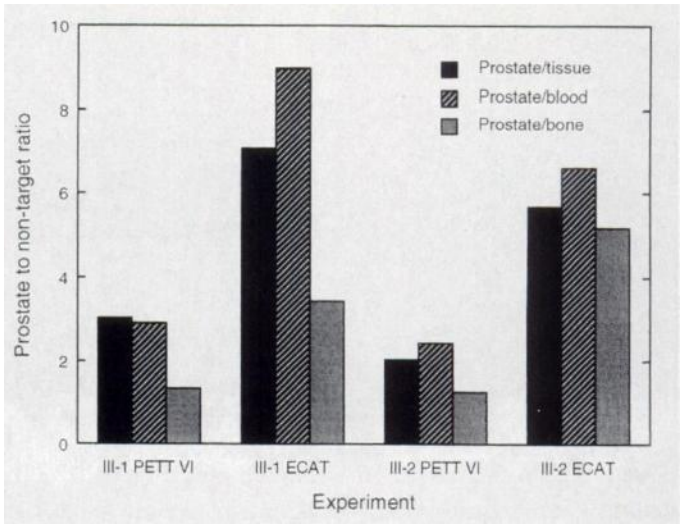

FIGURE 9. PETT VI versus Siemens/CTI ECAT 953b comparison of prostate to nontarget ratios at 1 hr postinjection of compound **III** in Baboons 1 and 2.

Approval by both the Human Studies Committee and the Radioactive Drug Research Committee of the Washington University School of Medicine has been obtained to begin this study. The present study has also shown the limitations of the rat model routinely used to evaluate radiolabeled androgens as imaging agents. The high bone uptake of compound **I** observed in the rat model was not seen in the primate. The study suggests an important role of SHBG in the metabolism and possibly the target tissue uptake of these radiolabeled steroids. This role needs to investigated further.

ACKNOWLEDGMENTS

Financial support was provided by the U.S. Department of Energy grants DE FG02 86ER60401 and DE FG02 84ER60218. We thank Kathryn E. Carlson for measurement of effective specific activities, John T. Hood, Jr. for operating the ECAT 953b scanner, Marcus E. Raichle for the use of the 953b, Terry L. Sharp for coordinating MR imaging and Deanna London for assistance in the preparation of the manuscript. This work was performed as part of a doctoral dissertation. A preliminary report of this work was presented at the 41st Annual Meeting of the Society of Nuclear Medicine in Orlando, Florida in 1994 (*70*).

REFERENCES

1. Wango PA, Tong T, Bolden S. Cancer statistics. *CA Cancer J Clin* 1995;45:8–30.
2. Blankenstein MA, Bolt-de Vries J, van Aubel OG, van Steenbrugge GJ. Hormone receptors in human prostate cancer. *Scan J Urol Nephrol* 1988;107:39–45.
3. Barrack ER, Tindall DJ. A critical evaluation of the use of androgen receptor assays to predict the androgen responsiveness of prostatic cancer. In: Coffey DS, ed. *Current concepts and approaches to the study of prostatic cancer.* New York, NY: Alan R. Liss; 1987:155–187.
4. Concolino G, Maroechi A, Margiotta G, et al. Steroid receptors and hormone responsiveness of human prostatic carcinoma. *Prostate* 1982;3:475–482.
5. Diamond DA, Barrack ER. The relationship of androgen receptor level to androgen responsiveness in the Dunning R3327 rat prostate tumor sublines. *Urology* 1984;132: 821–827.
6. Ekman P, Snochowski M, Dahlberg E, Gustafsson JÅ. Steroid receptors in metastatic carcinoma of the human prostate. *Eur J Can* 1979;15:257–262.
7. Ekman P, Snochowski M, Zetterberg A, Högberg B, Gustafsson JÅ. Steroid receptor content in human prostatic carcinoma and response to endocrine therapy. *Cancer* 1979;44:1173–1181.
8. Ekman P, Dahlberg E, Gustafsson JA, Högberg B, Pousette A, Snochowski M. Present and future clinical value of steroid receptor assays in human prostatic carcinoma. In: Lacobelli S, ed. *Hormones and cancer.* New York, NY: Raven Press; 1980;361–370.
9. Katzenellenbogen JA. The development of gamma-emitting hormone analogs as imaging agents for receptor-positive tumors. In: Murphy GP, Sandberg AA, eds. *The prostatic cell: structure and function part B.* New York, NY: Alan R. Liss; 1981:313–327.
10. Pertschuk LP, Rosenthall HE, Macchia RJ, et al. Correlation of histochemical and biochemical analysis of androgen binding in prostatic cancer: relation to therapeutic response. *Cancer* 1982;49:984–993.

11. Mobbs BG, Johnson IE. Basal and estrogen-stimulated hormone receptor profiles in four R3327 rat prostatic carcinoma sublines in relation to histopathology and androgen sensitivity. *Cancer Res* 1988;48:3077–3083.
12. Müntzing J, Kirdani RY, Murphy GP, Sandberg AA. A rat prostatic adenocarcinoma as a model for the human disease. *Invest Urol* 1979;17:37–41.
13. Trapma J, Stalpers CR, van der Korput JAGM, Kuiper GGJM, Brinkmann AO. The androgen receptor: functional structure and expression in transplanted human prostate tumors and prostate cell lines. *J Steroid Biochem Mol Biol* 1990;37:837–842.
14. Sadi MV, Barrack ER. Image analysis of androgen receptor immunostaining in metastatic prostate cancer: heterogeneity as a predictor of response to hormonal therapy. *Cancer* 1993;71:2574–2580.
15. Neri R. Pharmacology and pharmacokinetics of flutamide. *Urology* 1989;34(suppl): 19–21.
16. Mobbs BG, Johnson IE, Connolly JG. The effect of therapy on the concentration and occupancy of androgen receptors in the human prostatic cytosol. *Prostate* 1980;1:37–51.
17. Mobbs BG, Johnson JE, Connolly JG, Thompson J. Concentration and cellular distribution of androgen receptor in human prostatic neoplasia: can estrogen treatment increase androgen receptor content? *J Steroid Biochem* 1983;19:1279–1289.
18. Mobbs BG, Johnson IE. Increased androgen binding capacity in experimental prostatic carcinomas treated with estrogen. *Prog Cancer Res Therapy* 1984;31:467–476.
19. Karr JP, Wajsman Z, Madajewicz S, Kurdani RY, Murphy GP, Sandberg AA. Steroid hormone receptors in the prostate. *J Urol* 1979;122:170–175.
20. Motta M. In: Denis L, ed. *The endocrinological basis for hormonal therapy of prostate tumors. The medical management of prostate cancer II,* Berlin, Germany: Springer-Verlag; 1991;27–44.
21. Visakorpi T, Hyytinen E, Koivisto P, et al. In vivo amplication of the androgen receptor gene and progression of human prostate cancer. *Nature Genetics* 1995;9:401–406.
22. Choe YS, Lidström PJ, Chi DY, Bonasera TA, Welch MJ, Katzenellenbogen JA. Synthesis of 11β-[^{18}F]fluoro-5α-dihydrotestosterone and 11β-[^{18}F]fluoro-19-nor-5α-dihydrotestosterone: preparation via halofluorination-reduction, receptor binding and tissue distribution. *J Med Chem* 1995;38:816–825.
23. Liu A, Katzenellenbogen JA, VanBrocklin HF, Mathias CJ, Welch MJ. 20-[^{18}F]Fluoromibolerone, a positron-emitting radiotracer for androgen receptors: synthesis and tissue distribution studies. *J Nucl Med* 1991;32:81–88.
24. Liu A, Dence CS, Welch MJ, Katzenellenbogen JA. Fluorine-18-labeled androgens: radiochemical synthesis and tissue distribution studies on six fluorine-substituted androgens, potential imaging agents for prostatic cancer. *J Nucl Med* 1992;33:724–734.
25. Reiffers S, Vaalburg W, Weigman T, Wynberg H, Woldring MG. Carbon-11-labeled methyllithium as methyl donating agent: the addition to 17-keto steroids. *Int J Appl Radiat Isot* 1980;31:535–539.
26. Berger G, Maziere M, Prenant C, Sastre J, Comar D. Synthesis of high specific activity ^{11}C-17α-methyltestosterone. *Int J Appl Radiat Isot* 1981;32:811–815.
27. Ghanadian R, Waters SL, Chisholm GD. Investigations into the use of ^{77}Br-labeled 5α-dihydrotestosterone for scanning of the prostate. *Eur J Nucl Med* 1977;2:155–157.
28. Eakins MN, Waters SL. Synthesis of bromine-77-labeled 5α-dihydrotestosterone and a comparison of its distribution in rats with bromine-77-bromide. *Int J Appl Radiat Isot* 1979;30:701–704.
29. Hample R, Horakova J, Bickova M, Dvorak P, Starka L. Iodo derivatives of testosterone as potential biological markers. *J Steroid Biochem* 1980;13:1035–1038.
30. Hoyte RM, Rosner W, Hochberg RB. Synthesis of 16α-[^{125}I]-iodo-5α-dihydrotestosterone and evaluation of its affinity for the androgen receptor. *J Steroid Biochem* 1982;16:621–628.
31. Hoyte RM, MacLusky NJ, Hochberg RB. The synthesis and testing of E-17α-(2-iodovinyl)-5α-dihydrotestosterone and Z-17α-(2-iodovinyl)-5α-dihydrotestosterone as gamma-emitting ligands for the androgen receptor. *J Steroid Biochem* 1990;36:125–132.
32. Hoyte RM, Borderon K, Bryson K, Allen R, Hochberg RB, Brown TJ. Synthesis and evaluation of 7α-iodo-5α-dihydrotestosterone as a potential radioligand for the androgen receptor. *J Med Chem* 1994;37:1224–1230.
33. Tarle M, Padovan R, Spaventi S. The uptake of radioiodinated 5-alpha-dihydrotestosterone by the prostate of intact and castrated rats. *Eur J Nucl Med* 1981;6:79–83.
34. Skinner RWS, Pozerac RV, Counsell RE, Hsu CF, Weinhold PA. Androgen receptor binding properties and tissue distribution of 2-selena-A-nor-5α-androstan-17β-ol in the rat. *Steroids* 1977;30:15–23.
35. Carlson KE, Katzenellenbogen JA. A comparative study of the selectivity and efficiency of target tissue uptake of five tritium-labeled androgens in the rat. *J Steroid Biochem* 1990;36:549–561.
36. Brolin J, Skoog L, Ekman P. Immunohistochemistry and biochemistry in detection of androgen, progesterone and estrogen receptors in benign and malignant human prostatic tissue. *Prostate* 1992;20:281–295.
37. Kumar VL, Wadhwa SN, Kumar V, Farooq A. Androgen, estrogen and progesterone receptor contents and serum hormone profiles in patients with benign hypertrophy and carcinoma of the prostate. *J Surg Oncol* 1990;44:122–128.
38. Young JDJ, Sidh SM, Bashirelahi N. The role of estrogen, androgen and progestogen receptors in the management of carcinoma of the prostate. *Trans Amer Assoc Gen-Urin Surg* 1979;71:23–25.
39. Gustafsson JÅ, Ekman P, Pousette A, Snochowski M, Hogberg B. Demonstration of a progestin receptor in human benign prostatic hyperplasia and prostatic carcinoma. *Invest Urol* 1978;15:361–366.
40. Hobbs CJ, Jones RE, Plymate SR. The effects of sex hormone binding globulin (SHBG) on testosterone transport into the cerebrospinal fluid. *J Steroid Biochem Mol Biol* 1992;42:629–635.
41. Reventos J, Sullivan PM, Joseph DR, Gordon JW. Tissue-specific expression of the rat androgen-binding protein/sex hormone-binding globulin gene in transgenic mice. *Mol Cellular Endocrin* 1993;96:69–73.
42. Brandes SJ, Katzenellenbogen JA. Fluorinated androgens and progestins: molecular probes for androgen and progesterone receptors with potential use in positron emission tomography. *Mol Pharmacol* 1987;32:391–403.
43. Liu A, Carlson KE, Katzenellenbogen JA. Synthesis of high affinity fluorine-substituted ligands for the androgen receptor. Potential agents for imaging prostatic cancer by positron emission tomography. *J Med Chem* 1992;35:2113–2129.
44. Tait JF, Tait SAS. The effect of plasma protein binding on the metabolism of steroid hormones. *J Endocrinol* 1991;131:339–357.
45. Noé G, Cheng YC, Dabiké M, Croxatto HB. Tissue uptake of human sex hormone-binding globulin and its influence on ligand kinetics in the adult female rat. *Biol Reprod* 1992;47:970–976.
46. Krupenko SA, Krupenko NI, Danzo BJ. Interaction of sex hormone-binding globulin with plasma membranes from the rat epididymis and other tissues. *J Steroid Biochem Mol Biol* 1994;51:115–124.
47. Porto CS, Abreu LC, Gunsalus GL, Bardin CW. Binding of sex hormone-binding globulin (SHBG) to testicular membranes and solubilized receptors. *Mol Cellular Endocrin* 1992;89:33–38.
48. Shiina H, Ishibe T, Usui T. Interaction of testosterone-oestradiol binding globulin (TeBG) and albumin with human prostatic carcinoma in vitro. *Int J Urol Nephrol* 1993;25:577–582.
49. Müntzing J, Myhrberg H, Saroff J, Sandberg AA, Murphy GP. Histochemical and ultrastructural study of prostatic tissue from baboons treated with antiprostatic drugs. *Invest Urol* 1976;14:162–167.
50. Kaack B, Lewis RW, Resnick MI, Roberts JA. Biochemistry of the nonhuman primate prostate and seminal vesicles. I. Some chemical parameters. *Arch Androl* 1983;11: 123–129.
51. Kiesewetter DO, Kilbourn MR, Landvatter SW, Heiman DF, Katzenellenbogen JA, Welch MJ. Preparation of four fluorine-18-labeled estrogens and their selective uptakes in target tissues of immature rats. *J Nucl Med* 1984;25:1212–1221.
52. Senderoff SG, McElvany KD, Carlson KE, Heiman DF, Katzenellenbogen JA, Welch MJ. Methodology for the synthesis and specific activity determination of 16α-[^{77}Br]-bromoestradiol and 16α-[^{77}Br]-11β-methoxyestradiol, two estrogen receptor-binding radiopharmaceuticals. *Int J Appl Radiat Isot* 1982;33:545–551.
53. Welch MJ, Kilbourn MR. A remote system for the routine production of oxygen-15 radiopharmaceuticals. *J Label Cmpds Radiopharm* 1985;22:1193–1200.
54. Yamamoto M, Ficke DC, Ter-Pogossian MM. Performance study of PETT VI, a positron computed tomograph with 288 cesium fluoride detectors. *IEEE Trans Nucl Sci* 1982;NS-29:529–533.
55. Ter-Pogossian MM, Ficke DC, Hood JT Sr, Yamamoto M, Mullani NA. PETT VI: a positron emission tomograph utilizing cesium fluoride scintillation detectors. *J Comput Assist Tomogr* 1982;6:125–133.
56. Bergmann SR, Herrero P, Markham J, Weinheimer CJ, Walsh MN. Noninvasive quantitation of myocardial blood flow in human subjects with oxygen-15-labeled water and positron emission tomography. *J Am Coll Cardiol* 1989;14:639–652.
57. Sorenson JA, Phelps ME. *Physics in nuclear medicine,* 2nd ed. Philadelphia, PA: W.B. Saunders Corp.; 1987, 406–408.
58. Kubota K, Matsuzawa T, Ito M, et al. Lung tumor imaging by positron emission tomography using C-11 I-methionine. *J Nucl Med* 1985;26:37–42.
59. Swindler DR, Wood CD. *An atlas of primate gross anatomy.* Seattle, WA: University of Washington Press; 1973:370.
60. Schmidt TJ, Visek WJ. Sucrose density gradient characterization of cytoplasmic [1,2-^{3}H]-5α-dihydrotestosterone binding proteins in the accessory sexual glands of the male Syrian hamster. *J Steroid Biochem* 1978;9:317–324.
61. Takane KK, Husmann DA, McPhaul MJ, Wilson JD. Androgen receptor levels in the rat penis are controlled differently in distinctive cell types. *J Urol* 1991;128:2234–2238.
62. Nonomura K, Sakakibara N, Demura T, Mori T, Koyanagi T. Androgen binding activity in the spongy tissue of mammalian penis. *J Urol* 1990;144:152–155.
63. Pomper MG, VanBrocklin HF, Thieme AM, et al. 11β-Methoxy-, 11β-ethyl- and 17α-ethynyl-substituted 16α-fluoroestradiols: receptor-based imaging agents with enhanced uptake efficiency and selectivity. *J Med Chem* 1990;33:3143–3155.
64. VanBrocklin HF, Rocque PA, Lee HV, Carlson KE, Katzenellenbogen JA, Welch MJ. 16β-[^{18}F]fluoromoxestrol: a potent, metabolically stable positron emission tomography imaging agent for estrogen receptor positive human breast tumors. *Life Sci* 1993;53:811–819.
65. Kiesewetter DO, Katzenellenbogen JA, Kilbourn MR, Welch MJ. Synthesis of 16-fluoroestrogens by unusually facile fluoride ion displacement reactions: prospects for the preparation of fluorine-18-labeled estrogens. *J Org Chem* 1984;49:4900–4905.
66. Dehdashti F, Mortimer JE, Siegel BA, et al. Positron tomographic assessment of estrogen receptors in breast cancer: comparison with FDG-PET and in vitro receptor assays. *J Nucl Med* 1995;36:1766–1774.
67. McGuire AH, Dehdashti F, Siegel BA, et al. Positron tomographic assessment of 16α-[^{18}F]fluoro-17β-estradiol uptake in metastatic breast carcinoma. *J Nucl Med* 1991;32:1526–1531.
68. Mintun MA, Welch MJ, Siegel BA, et al. Breast cancer: PET imaging of estrogen receptors. *Radiology* 1988;169:45–48.
69. Wagner RK. Extracellular and intracellular steroid binding proteins. Properties, discrimination, assay and clinical applications. *Acta Endocrinol* 1978;88:1–73.
70. Bonasera TA, O'Neil JP, Choe YS, et al. Imaging the prostate in baboons with fluorine-18-labeled androgen receptor ligands. *J Nucl Med* 1994;35:53P.